3.5.6

Instrument Developments and Neutron Brillouin Scattering Experiments on HRC

Shinichi Itoh[1], Tetsuya Yokoo[1], Takatsugu Masuda[2], Hideki Yoshizawa[2], Minoru Soda[2], Yoichi Ikeda[2], Soshi Ibuka[1], Toshio Asami[2], Ryosuke Sugiura[2], Daichi Kawana[2], Tomoko Shinozaki[2], and Yoshiaki Ihata[3]

[1]Neutron Science Division, Institute of Materials Structure Science, High Energy Accelerator Research Organization, Tsukuba, Ibaraki 305-0801, Japan
[2]Neutron Science Laboratory, The Institute for Solid State Physics, The University of Tokyo, Tokai, Ibaraki 319-1106, Japan
[3]Technology Development Section, Materials and Life Science Experimental Facility, J-PARC Center, Tokai, Ibaraki 319-1195, Japan

E-mail: shinichi.itoh@kek.jp

Abstract. To study condensed-matter dynamics over a wide energy-momentum space with high resolutions, the High Resolution Chopper Spectrometer (HRC) was installed at BL12 in MLF/J-PARC. In the previous ICANS meeting, we reported the performance of the HRC after the initial construction. Since then, we made further developments on the instrumentation. In particular, neutron Brillouin scattering (NBS) experiments became feasible by reducing the background noise at low scattering angles.

1. Introduction

The High Resolution Chopper Spectrometer (HRC) was installed at the BL12 beam port in the Materials and Life Science Experimental Facility (MLF), the Japan Proton Accelerator Research Complex (J-PARC), in order to study dynamics in condensed matters with high-resolutions and relatively high-energy neutrons [1, 2, 3]. A schematic layout of the HRC is illustrated in Fig. 1. The HRC faces the decoupled moderator which emits neutrons with sharp pulses. The sample is mounted at $L_1 = 15$ m from the moderator. On the primary flight path from the neutron source to the sample, some devices are mounted to control the incident neutron beam: a supermirror guide tube to increase the neutron flux, a T0 chopper to eliminate background noise originated by the initial burst of high energy neutrons, a Fermi chopper to monochromatize the incident beam and to control the resolution and the neutron flux, and an incident beam collimator system to reduce background noise due to unwanted scattering. An array of position sensitive detectors (PSDs) is located at $L_2 = 4$ m from the sample covering the scattering angles between $\phi = 3^\circ$ and 42° horizontally and $\pm 20^\circ$ vertically for conventional experiments. Another array of PSDs is located at $L_2 = 5.2$ m down to $\phi = 0.5^\circ$ for neutron Brillouin scattering (NBS) experiments. We confirmed that, under limited conditions, the neutron intensity and the energy resolution were in good agreement with the design values [1]. We here describe further instrument developments as well as success in the NBS experiments.

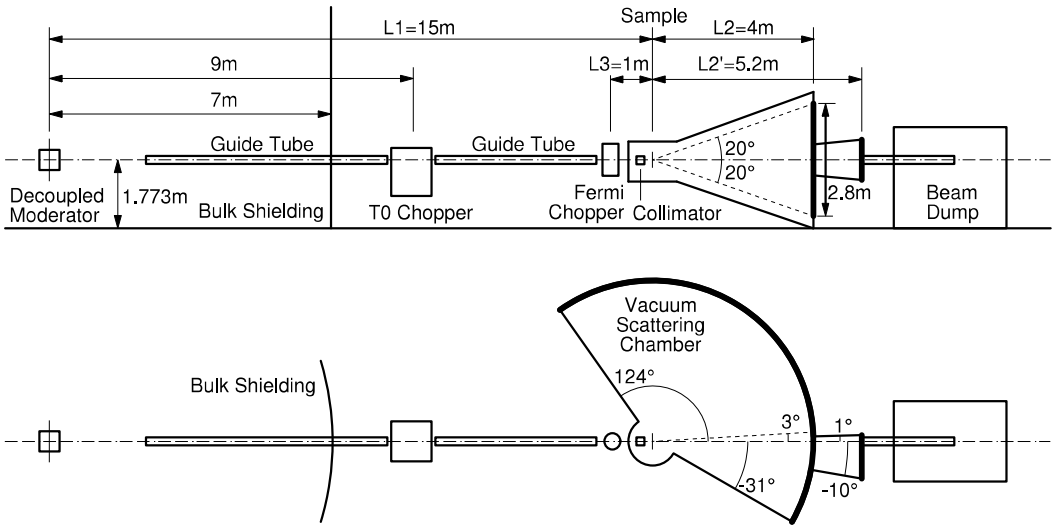

Figure 1. Schematic layout of the HRC, a side view (upper) and a top view (lower). Thick lines indicate PSDs to be mounted.

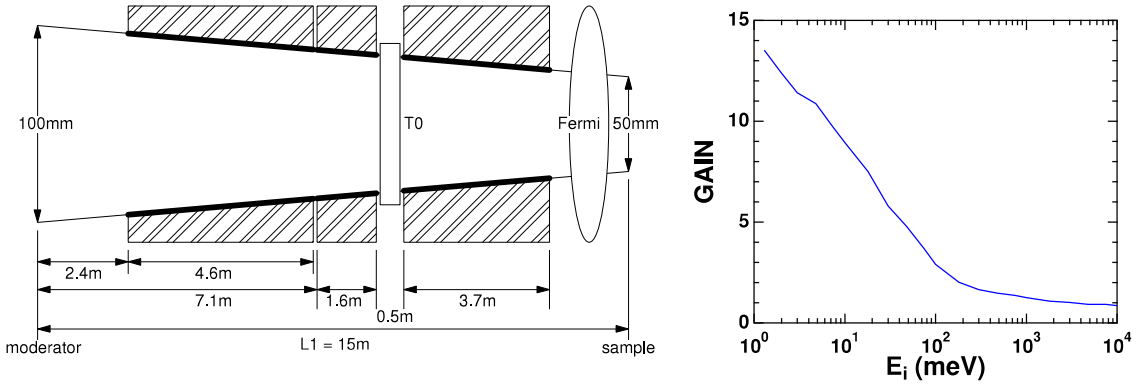

Figure 2. Scehmatic layout of the supermirror guide tube (thick lines) in the primary flight path (left), and observed gain of the supermirror guide system on the HRC in comparison with the previous setup where only the upstream section of 4.6 m was installed (right).

2. Instrument Developments

Since the above initial construction, we have continuously improved the HRC at many points as described below. In particular, by the installation of the collimator system to reduce background, the NBS experiments have been feasible on HRC.

2.1. Supermirror Guide Tube

On the primary flight path of $L_1 = 15$ m, the supermirror guide tube was initially installed only in the shutter and the biological-shielding sections of 4.6 m, and the collimator tube was in the downstream section of 5.3 m, in the initial construction. After that, the collimator tube was replaced by a supermirror guide tube of 5.3 m [4]. By this installation, we obtained a great intensity gain, as shown in Fig. 2.

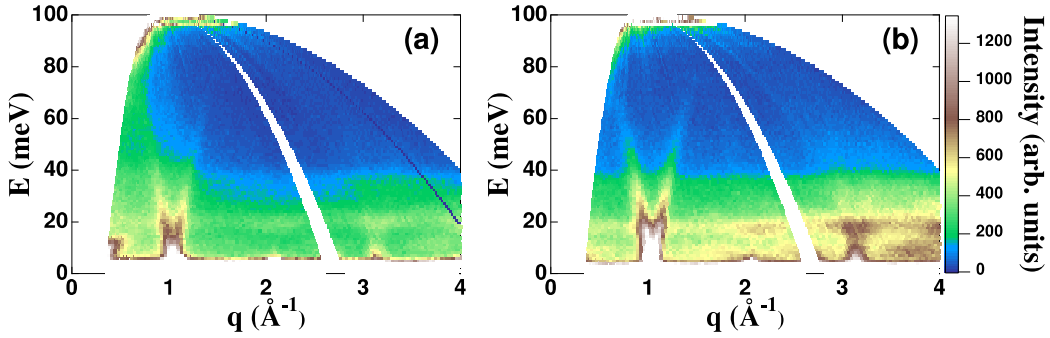

Figure 3. Excitation spectrum from $CsVCl_3$ measured with $E_i = 102$ meV, without a collimator system and an initial guide tube system (a), and with the 2.3° collimator and the full guide tube system (b). The intensities are normalized by the number of protons incident to the neutron production target. The noise at low-q has been greatly reduced by the 2.3° collimator, also the neutron flux has been increased by the installation of the guide tube.

2.2. Collimator System

A Soller collimator system composed of slits of vertical sheets of Cd with a thickness of 0.1 mm was installed just upstream of the sample. We can automatically select one of the two collimators with the collimation of 2.3° or 0.6° [4].

Since there was a huge background noise at low angles, as shown in Fig. 3 (left), a measurement with an empty can was required. Figure 3 shows excitation spectra in a one-dimensional antiferromanget, $CsVCl_3$, measured at 20 K. By using the 2.3° collimator, the background at low angles was greatly reduced and a spectrum from the sample can be obtained without an empty scan, as shown in Fig. 3 (left).

In the lower angle region, PSDs are installed down to $\phi = 0.5°$. These low angle detectors as well as sub-eV incident neutrons enable the NBS experiments on the HRC [5]. Figure 4 shows observed spectra from an empty can at $\phi = 0.64°$ with the incident neutron energy of $E_i = 102$ meV. A spread of the direct beam at the energy transfer of $E = 0$ meV and a spurious peak at $E = 5$ meV were observed with the collimator with the 0.6° collimation. The direct beam spread was eliminated and the spurious peak was reduced by using the collimator with the 0.3° collimation. The spurious peak at $E = 5$ meV, originating from a reflection of the direct beam at a position near the PSDs, could be successfully eliminated by masking the position with a cadmium plate. Finally, based on these developments, 2.3° and 0.3° collimators were replaced by 1.5° and 0.2° collimators, respectively.

2.3. Computational Environment

An experimental control environment was developed to combine the measurements of neutron counts with the control of devices such as choppers, temperature controllers, goniometers, vacuum system, and so on, as shown in Fig. 5 [4]. The HRC Control Platform was developed and installed on the computer named DAQ-OP (DAQ operator). The HRC Device Control Software controls the devices as well as the DAQ middleware (DAQ MW) via the Control LAN through the Platform. The HRC Experiment Control Software executes a sequence composing begin/end of measurements and controls of devices. At present, almost all the devices on the HRC can be controlled through this platform and these operations can be connected with the data acquisition (begin/end of measurements). In order to optimize the computing environment, the composition of the computers was improved.

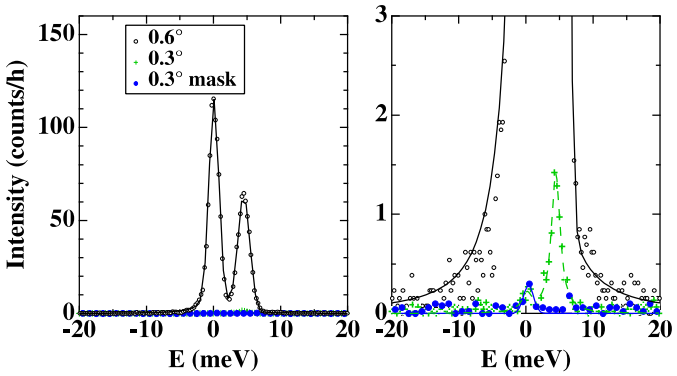

Figure 4. Background noise at $\phi = 0.64°$ for the 0.6°, the 0.3° collimators, and the 0.3° collimator with a cadmium mask at the position of the direct beam hit. The same data are plotted in both figures with different scales in the vertical axes. The lines are guides to the eye.

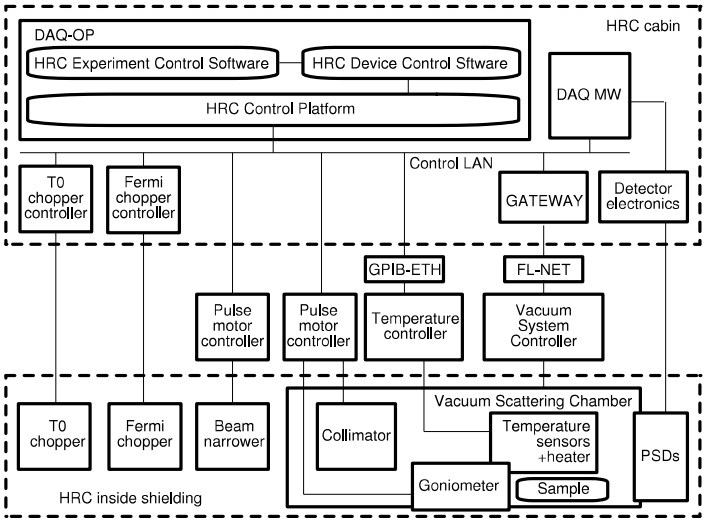

Figure 5. Experimental control environment on the HRC. GPIB-ETH represents a GPIB/Ethernet converter. The vacuum system is accessible through a Gateway server and an FL-net interface. The incident neutron beam is controlled by the T0 chopper, the Fermi chopper, the narrower, and the collimator. The sample environments such as the temperature and the crystal angle are controlled.

We also developed the software to analyze single crystal sample data as well as powder sample data. The analyzed data can be transformed to the standard Mslice format for a convenience of users. Also, the process for the alignment of the sample crystal became very easy. The excitation spectra in the three-dimensional system on the four-dimensional energy-momentum space can be also measured by rotating the crystal axis of the sample, and visualized.

2.4. Other Developments

Initially, we installed two Fermi chopper: one is a so-called sloppy chopper for high intensities and the other is optimized for $E_i = 200$ meV at 600 Hz with the optimum condition. Therefore,

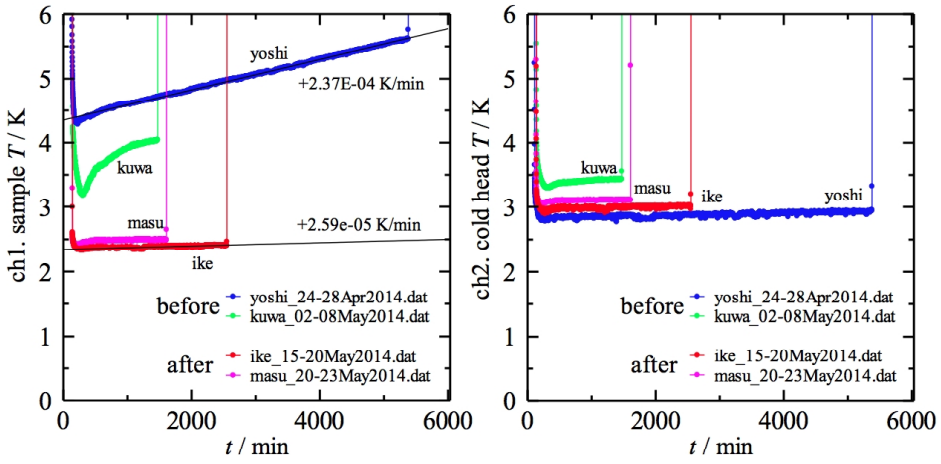

Figure 6. Temperature variations at the sample can (left) and the cold head of the refrigerator (right) before and after the improvement of the radiation shielding on the GM-type refrigerator.

the optimum condition, where the chopper open time is equivalent to the pulse width, was realized in the energy range of $E_i = 10 - 200$ meV. At present, we installed a Fermi chopper optimized for $E_i = 500$ meV at 600 Hz, and then the energy range for the optimum resolution of $\Delta E/E_i = 2.5$ - 3% was extended up to $E_i = 500$ meV [4].

In the initial construction, the sample area was separated from the vacuum scattering area near PSDs with a thin Al foil in the vacuum scattering chamber, and the sample area was evacuated by a small TMP (turbo molecular pump) to achieve a high vacuum for cooling down the sample. The TMP was replaced by a cryopump with a pumping speed of 28 m^3/s and the Al foil was removed. A gate valve with a diameter of 750 mm was also mounted between the cryopump and the chamber. A cryopump system is now used for evacuating the vacuum scattering chamber encompassing the sample and the flight path of the scattered neutrons. After installing this system, the regeneration process of the cryopump, which is the process to release absorbed molecules, was optimized and a frequency of the evacuation without the regeneration was greatly reduced.

For conventional experiments, 128 pieces of 2.8 m PSDs, which are mounted into two detector banks, covers $\phi = 3 - 42°$ at present. 64 pieces of 2.8m PSDs are mounted on each detector bank panel of 1.5 m × 3 m with a vacuum flange, and two panels with PSDs are hold on the vacuum scattering chamber. To remove the panel from the vacuum chamber, it was necessary to remove the shielding block above the vacuum scattering chamber first, and then, remove the panel by using a crane installed at the experimental hall. At present, we mounted a rail on the vacuum chamber body just above each panel, and the panel can be removed from the chamber along the rail by using a hand chain hoist. By using this mechanism, we replaced the damaged PSDs by new ones in a much easier procedure without removing the shielding.

We have a variety of sample environments: a GM type refrigerator, a ^{3}He sorption pumping type refrigerator, a ^{3}He circulation type refrigerator, and a cryomagnet. The GM-type refrigerator is conventionally used to cool the sample down to 4 K stably. This refrigerator shows a good cooling performance by improving the radiation shielding, which is made of thin Al foil and contacts to the cold head. The sample temperature down to 2.5 K and the heat-up rate of 26 μK/min on the sample have been confirmed, as shown in Fig. 6. A temperature sensor with a fine calibration is used at the sample, and that with a rough calibration is at the cold head. This may cause the higher temperature indication at the cold head for the best case indicated

by "*ike*" and "*masu*". Also, the lowest temperatures of 0.3 K and 0.6 K were confirmed for the ^{3}He sorption pumping type refrigerator and the ^{3}He circulation type refrigerator, respectively.

A cryomagnet to apply the magnetic field up to 14 T to the sample down to 0.3 K was introduced. We performed the commissioning at the Guide Hall of JRR-3M, and confirmed that it was successfully operated with the maximum magnetic field of 14 T at the lowest temperature of 0.3 K. Then we moved the cryomagnet to the HRC, and examined the maximum magnetic field in the actual setup of the experiments. We confirmed the maximum magnetic field of 10 T on the HRC without any damage to devices at around the sample area.

3. Neutron Brillouin Scattering Experiments

On the HRC, the NBS experiments became feasible by reducing the background noise at low scattering angles down to $\phi = 0.5°$. NBS is the most promising way to observe excitations in the forward direction from powders, polycrystals, or liquids. Owing to the kinematical constraints of neutron spectroscopy, E_i in the sub-eV region is necessary for measuring scattering in the meV range of E near to (000), and with a high energy resolution of $\Delta E/E_i$, further, the scattered neutrons need to be detected at very low ϕ. Low angle detectors are essential to access the present energy momentum space. In fact, the region above the dashed line in Fig. 7, which is the envelope of scan loci for $\phi = 5°$ with respect to E_i, can never be accessed using a conventional spectrometer with the lowest scattering angle of $\phi = 5°$, for instance.

3.1. Feasibility of NBS on HRC

First, NBS experiment was performed on the HRC to observe spin waves in a polycrystalline sample of a cubic perovskite, $La_{0.8}Sr_{0.2}MnO_3$, (Curie temperature: $T_C = 316$ K). Magnetic properties of this material are well elucidated and it has been already reported that spin waves were measured by using a single crystal sample. Figure 7 (a) shows the dispersion relation of spin waves in $La_{0.8}Sr_{0.2}MnO_3$ measured with $E_i = 102$ meV, where $\Delta E/E_i = 2\%$. The observed dispersion relations at 245 K was well fitted to $E = DQ^2$, where Q is the scattering vector. The D value was obtained to be 88 ± 2 meVÅ^2 at 245 K. This value is in good agreement with the results ($D = 89$ meVÅ^2 at 250 K) obtained by the previous experiments using a single crystal [8, 9]. Therefore, the feasibility of NBS experiments on the HRC was demonstrated [5, 6, 7].

3.2. Spin dynamics in metallic ferromagnet $SrRuO_3$

Spin waves in a polycrystalline ferromagnet $SrRuO_3$ ($T_C \sim 160$ K) were measured, because a large single crystal suitable for inelastic neutron scattering experiments has not yet been synthesized. This material has recently become attractive because of an enhanced anomalous Hall effect due to the robust spin-orbit coupling of the Ru 4d orbital [10]. The measurement was performed at 7 K with $E_i = 102$ meV, and well-defined spin wave peaks were observed. As shown in Fig. 7 (a), the dispersion relation of spin waves in $SrRuO_3$ was well fitted to $E(Q) = E_g + DQ^2$ with an apparent energy gap E_g [6]. Also, the temperature (T) dependence of D and E_g was investigated. We found that $D(T)$ was almost independent of T up to T_C, and $E_g(T)$ could be related to the anomalous Hall conductivity. These results might suggest the intermediate electron correlation in $SrRuO_3$ as well as the vital role of magnetic monopoles in momentum-space as a source of strong Berry curvature originating from the spin-orbit interaction [11].

3.3. Spin waves in permanent magnet $Nd_2Fe_{14}{}^{11}B$

$Nd_2Fe_{14}B$ is a well-known song permanent magnet with $T_C = 580$ K and the saturation magnetization of 1.6 T. At room temperature, all spins are aligned along the c*-axis. Below 130 K the system exhibits a spin reorientation. Because the unit cell includes four chemical formulae of $Nd_2Fe_{14}B$ in a tetragonal lattice, spin-wave branches are expected to be complicated. In a

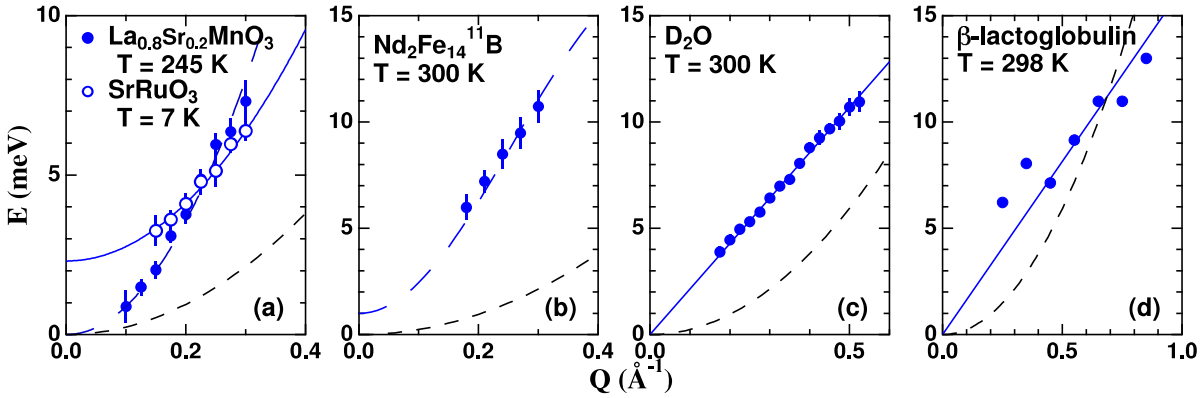

Figure 7. Dispersion relations obtained by the NBS on the HRC: spin waves in $La_{0.8}S_{r0.2}MnO_3$, $SrRuO_3$ (a) and in $Nd_2Fe_{14}{}^{11}B$ (b), phononic excitations in D_2O (c) and in β-lactoglobulin (d). The solid lines are fitted curves. The dashed lines are the dispersion relations reported previously. The region above the dotted black line in each figure, which is the envelope of scan loci for the scattering angle of 5° (the lowest angle for a conventional spectrometer) with respect to E_i, can never be accessed using a conventional spectrometer.

previous inelastic neutron scattering experiment using a single-crystalline sample of $Nd_2Fe_{14}{}^{11}B$, a spin-wave branch was detected only along the c*-axis around (002) at 6 and 295 K [12]. We performed NBS experiments in a $Nd_2Fe_{14}{}^{11}B$ polycrystalline sample at 6 and 300 K with E_i = 257 meV and ΔE = 5.7 meV [7, 13]. The observed spin-wave peaks at 300 K were well fitted to Gaussian scattering functions with widths determined from the resolution, and the peak positions were determined in Fig. 7 (b). The observed peak positions were on the dispersion curve along the c*-axis reported in the previous experiment using a single crystal [12]. No magnetic peaks were observed at 6 K, this result is also consistent with the reported dispersion at 6 K.

3.4. Phononic excitations in liquid D_2O

Phononic excitations in a liquid D_2O were measured at 300 K with E_i = 102 meV and ΔE = 2.0 meV [7]. The observed spectra showed broad excitation peaks and a resolution-limited elastic peak. The excitation peaks were fitted with a damped harmonic oscillator scattering function convoluted with the instrumental resolution width multiplied by a temperature factor and the peak positions $E(Q)$ were determined. The present analysis was identical to that for the previous inelastic neutron scattering experiment [14]. As shown in Fig. 7 (c), the Q dependence of the observed peak positions down to Q = 0.02 Å^{-1} was well fitted to $E(Q) = cQ$ with c = 21.4 ± 0.2 meV, which is equivalent to c = 3250 ± 30 m/s. The observed sound velocity c was in good agreement with that for the fast sound observed in the previous experiment with E_i = 80 meV and ΔE = 4.8 meV down to Q = 0.035 Å^{-1} [14].

3.5. Collective dynamics of hydrated β-lactoglobulin

Protein hydration plays a fundamental role in protein behavior: water-protein interactions affect protein folding, maintain structural integrity, mediate molecular recognition, and accelerate enzymatic catalysis. Many scattering measurements, both elastic and inelastic, and many molecular dynamics simulations, have been performed to investigate the relation between protein dynamics and that of the surrounding solvent molecules. Single particle dynamics of proteins and

hydrated water have been investigated using incoherent scattering from hydrogen in hydrated protein powder. On the other hand, the investigation of collective dynamics of proteins and hydrated water using coherent scattering is relatively scarce, although it contains important information of structure and dynamics. First, we performed NBS experiment of pure D_2O at room temperature on the HRC, as mentioned above. The fast sound mode due to the collective dynamics of water was detected. Next, hydrated β-lactoglobulin powder was measured at 180 - 298 K. The inelastic neutron scattering spectra show well-defined acoustic excitations that change in excitation energy with Q in the low Q region. The obtained dispersion relation is shown in Fig. 7 (d) and the high-frequency sound velocity was almost independent of the temperature and was 2460 $\pm$ 110 m/s at 298 K [15].

4. Summary

Since the initial construction, we have continuously improved the HRC at many points. We believe that the HRC shows the best performance based on the present technology. In particular, by the installation of the collimator system to reduce background, NBS experiments have been feasible on the HRC. The NBS is the promising way to observed coherent excitations in powder, polycrystalline, noncrystalline and liquid systems. In the current research in material science, most of the newly synthesized materials are chemically and structurally complicated such that large single crystals are not always possible to be synthesized. NBS experiments on the HRC bring about new opportunities to such material development.

Acknowledgments

This neutron scattering experiments were approved by the Neutron Scattering Program Advisory Committee of the Institute of Materials Structure Science, High Energy Accelerator Research Organization (Proposal Nos. 2012S01, 2013S01 and 2014S01). The NBS experiments were conducted in collaboration with Y. Endoh, M. Fujita, Y. Kaneko, Y. Tokura, K. Ono, K. Saito, N. Inami, and K. Yoshida.

References

[1] Itoh S, Yokoo T, Satoh S, Yano S, Kawana D, Suzuki J and Sato S J 2011 *Nucl. Instr. Meth. Phys. Res.* A **631** 90
[2] Yano S, Itoh S, Satoh S, Yokoo T, Kawana D and Sato T J 2011 *Nucl. Instr. Meth. Phys. Res.* A **654** 421
[3] Itoh S, Yokoo T, Kawana D, Yano S, Satoh S, Sato T J, Masuda T, Yoshizawa H 2012 *Proc. 20th Meeting of the International Collaboration on Advanced Neutron (ICANS-XX)* (Centro Atomico Bariloche) p 416
[4] Itoh S, Yokoo T, Kawana D, Yoshizawa H, Masuda T, Soda M, Sato T J, Satoh S, Sakaguchi M and Muto S 2013 *J. Phys. Soc. Jpn.* **82** SA033
[5] Itoh S, Yokoo T, Kawana D and Endoh Y 2013 *J. Phys. Soc. Jpn.* **82** SA034
[6] Itoh S, Endoh Y, Yokoo T, Kawana D, Kaneko Y, Tokura Y and Fujita M 2013 *J. Phys. Soc. Jpn.* **82** 043001
[7] Itoh S, Yokoo T, Kawana D, Kaneko Y, Tokura Y, Fujita M, Yoshida K, Saito K, Inami N, Takeichi Y, Ono K, Endoh Y 2014 *J. Phys.: Conf. Series* **502** 012043
[8] Endoh Y and Hirota K 1997 *J. Phys. Soc. Jpn.* **66** 2264
[9] Moussa F, Hennion M, Kober-Lehouelleur P, Reznik D, Petit S, Moudden H, Ivanov A, Mukovskii Y M, Privezentsev R and Albenque-Rullier F 2007 *Phys. Rev. B* **76** 064403
[10] Fang Z, Nagaosa N, Takahashi K S, Asamitsu A, Mathieu R, Ogasawara T, Yamada H, Kawasaki M, Tokura Y and Terakura K 2003 *Science* **302** 92
[11] Itoh S, Endoh Y, Yokoo T, Park J-G, Kaneko Y, Tokura Y, Nagaosa N 2014 *unpublished*
[12] Mayer H M, Steiner M, Stüßer N, Weinfurter H, Kakurai K, Doner B, Lindgård P A, Clausen K N, Hock S, Rodewald W 1991 *J. Magn. Magn. Matter.* **97** 210
[13] Ono K, Inami N, Saito K, Takeichi Y, Yano M, Shoji T, Manabe A, Kato A, Kaneko Y, Kawana D, Yokoo T and Itoh S 2014 *J. Appl. Phys.* **115** 17A714
[14] Teixeira J, Bellissent-Funel M C, Chen S H, Dorner B 1985 *Phys. Rev. Lett.* **54** 2681
[15] Yoshida K, Yamaguchi T, Kawana D, Yokoo T and Itoh S 2014 *MLF Annual Report 2013* (J-PARC Center) *in press*